Dalton Transactions

PAPER

View Article Online
View Journal | View Issue

Cite this: *Dalton Trans.*, 2019, **48**, 13440

Complex formation between UO_2^{2+} and α-isosaccharinic acid: insights on a molecular level†

Hannes Brinkmann, *[a] Michael Patzschke, [a] Peter Kaden, [a] Manuel Raiwa,[b] André Rossberg,[a,c] Roger Kloditz,[a] Karsten Heim,[a] Henry Moll [a] and Thorsten Stumpf[a]

Cellulosic materials present as tissue, paper, wood, or filter materials in low and intermediate level waste will degrade under alkaline conditions if water ingresses in a cementitious backfilled repository. The main degradation product is isosaccharinic acid. Complex formation with isosaccharinic acid may adversely affect the retention of radionuclides by the sorption or formation of solid phases. Hence, this compound is of particular concern in the context of nuclear waste disposal. Structural information of complexes is limited to spherical metal centers and little is known about the interaction of uranyl ($U^{VI}O_2^{2+}$) with isosaccharinic acid. Therefore, the interaction of UO_2^{2+} with α-isosaccharinate (ISA) was studied under acidic conditions focusing particularly on the structural characterization of the formed complexes. Attenuated total reflection Fourier-transform infrared (ATR-FTIR), nuclear magnetic resonance (NMR), UV-Vis, extended X-ray absorption fine structure (EXAFS) spectroscopy and electrospray-ionization mass spectrometry (ESI-MS) were combined with theoretical calculations to obtain a process understanding on the molecular level. The dominant binding motifs in the formed complexes are 5- and 6-membered rings involving the carboxylic group as well as the α- or β-hydroxy group of ISA. Two concentration dependent complex formation mechanisms were identified involving either mono- ($[UO_2(ISA)(H_2O)_3]^+$) or binuclear ($[(UO_2)_2(ISA)(H_2O)_6]^{3+}$) species. Furthermore, this study unveils the interaction of UO_2^{2+} with the protonated α-isosaccharinic acid (HISA) promoting its transformation to the corresponding α-isosaccharinate-1,4-lactone (ISL) and inhibiting the formation of polynuclear UO_2^{2+}–ISA species. Future studies on related systems will benefit from the comprehensive knowledge concerning the behavior of ISA as a complexing agent gained in the present study.

Received 12th March 2019,
Accepted 22nd July 2019

DOI: 10.1039/c9dt01080g

rsc.li/dalton

1 Introduction

Energy production by nuclear power plants and the use of radioactive materials for military, industrial, and medical applications generates nuclear waste. To ensure its safe isolation from the biosphere as well as to minimize the potential risk for humans and the environment of being exposed to harmful compounds, the nuclear waste will be stored in deep geological facilities. Therefore, suitable containers confining the conditioned waste will be collected in vaults and stored in stable host rock formations. Cementitious materials can be used to backfill the remaining cavities providing a physical and chemical barrier to radionuclide release. Additionally, cement-based materials serve as construction materials and for waste conditioning purposes. The ingress of groundwater will promote the degradation of cementitious materials, consequently leading to the development of alkaline conditions, which will in turn impact the chemical composition of the waste and the speciation of radionuclides.[1]

The largest proportion of nuclear waste in terms of volume consists of low and intermediate level waste (LILW). Amongst others, it contains different types of organic polymers like ion exchange resins, halogenated and non-halogenated plastics, rubber, and cellulosic materials. The latter, which are introduced as paper, cotton, tissue, wood, or filter materials, are not stable under alkaline conditions and will degrade to water-soluble, low-molecular-weight organic compounds known as cellulose degradation products (CDPs) with isosaccharinic acid

[a]*Helmholtz-Zentrum Dresden – Rossendorf, Institute of Resource Ecology, Bautzner Landstraße 400, 01328 Dresden, Germany. E-mail: h.brinkmann@hzdr.de, m.patzschke@hzdr.de, p.kaden@hzdr.de, r.kloditz@hzdr.de, k.heim@hzdr.de, h.moll@hzdr.de, t.stumpf@hzdr.de*
[b]*Gottfried Wilhelm Leibniz Universität Hannover, Institute of Radioecology and Radiation Protection, Herrenhäuser Str. 2, 30419 Hannover, Germany. E-mail: raiwa@irs.uni-hannover.de*
[c]*ESRF European Synchrotron, Rossendorf Beamline, CS40220, F-38043 Grenoble, France. E-mail: rossberg@esrf.fr*

†Electronic supplementary information (ESI) available. See DOI: 10.1039/c9dt01080g

as a main degradation product.[2–8] Studies related to the impact of CDPs on the sorption or solubility of RN and other metals relevant in the context of nuclear waste disposal showed that they have an adverse effect while isosaccharinic acid was identified as a responsible complexing agent in many cases.[9–13] Hence, this particular organic ligand is of great concern in the context of safety assessment for a nuclear waste repository. Extensive efforts have been made to understand this behavior. This is reflected in the number of studies related to the effect of isosaccharinic acid on the sorption or solubility of RN and other metals. Hummel *et al.* provided a summary of the related literature up to the year of 2004.[15] Gaona *et al.* and Rai and Kitamura provided comprehensive and critical summaries of studies.[16,17] Recently, Tasi *et al.* reported new insights concerning the interaction of isosaccharinic acid with plutonium while they also provided a detailed overview of experimental studies related to the complexation of that ligand with tri- and tetravalent actinides and lanthanides.[18,19]

Two diastereomers (α- and β-form) of isosaccharinic acid form in similar quantities.[4] However, most studies focused on α-isosaccharinic acid since its synthesis is well described in the literature. Furthermore, Van Loon and Glaus observed a stronger complexation for certain metals compared to the β-form.[14] α-Isosaccharinic acid is a polyhydroxy-carboxylic acid with four alcohol functionalities (structures are shown in Fig. 1; the following abbreviations will be used throughout the remaining article: ISL for α-isosaccharinate-1,4-lactone, HISA for α-isosaccharinic acid and ISA for α-isosaccharinate). Under very acidic conditions ISL dominates while the transformation from HISA *via* a proton catalyzed dehydration is a rather slow reaction.[6,20–23] The ring closure occurs between the carboxylic carbon (C_1) and the secondary alcohol (C_4–OH) resulting in a γ-lactone. Equilibrium constants for deprotonation and lactonization were recently evaluated by Rai and Kitamura.[24] The pK_a value of the carboxylic group is 3.27 while the deprotonation of alcohol functionalities is expected to occur above pH 12.[23,25,26] However, the acidity of alcohol functionalities is expected to increase upon their interaction with Lewis acidic metal centers.[23,27] The previously mentioned impact of ISA on the sorption and solubility was generally traced back to the formation of strong complexes in which the hydroxyl groups of the ligand in addition to the carboxylic group play a crucial role. However, while the stoichiometry of the expected complexes can be deduced from the sorption or solubility data, the structural properties and binding motifs were usually assumed. As stated by Randall *et al.*, comprehensive understanding of the structure of the formed complexes is crucial, since the sensitivity of complexation to changing parameters such as pH or ligand concentrations can be confidently understood, if the underlying structure and the structural changes of the dominant complexes are known.[10]

EXAFS measurements in the Th(IV)–ISA system performed by Colàs suggested the coordination of one or more hydroxyl groups while they showed no indication for a bidentate coordination of the carboxylic group.[28] NMR-measurements from Dudás *et al.* revealed that ISA acts as a multidentate ligand for Ca(II) under alkaline conditions.[26] They suggested the coordination *via* the carboxylic group as well as the tertiary alcohol (C_2–OH) and the secondary alcohol (C_4–OH), of which one is deprotonated. Furthermore, the authors concluded that the primary alcohol in the β-position (C_6–OH) to the carboxylic group is not involved in complex formation. Similar conclusions were drawn by Randall *et al.* based on NMR investigations in the Eu(III)–ISA system.[10] A coordination of Eu(III) by the carboxylic group, the secondary alcohol (C_4–OH) and the tertiary alcohol (C_2–OH) was proposed. Based on the experimental results in combination with DFT-calculations, Tasi *et al.* identified the same functional groups involved in Pu(IV) complexation under alkaline conditions.[18] These findings reveal a coherent picture for the coordination of spherical metal centers nested in a pocket of oxygen atoms from the carboxylic group, and the secondary and tertiary alcohols. However, experimental data for hexavalent actinides possessing a sterically demanding structure with two linearly arranged oxygen atoms are scarce. Rao *et al.* characterized the uranyl ($U^{VI}O_2^{2+}$, hereafter referred to as UO_2^{2+})–ISA systems under acidic conditions by potentiometry and calorimetry.[29] Their potentiometric measurements suggested the formation of $[UO_2(ISA)_n]^{2-n}$ complexes with n = 1, 2 and 3. The same system was investigated by Warwick *et al.* under neutral and alkaline conditions.[30] The formation of UO_2^{2+}–ISA complexes with a 1-to-1 stoichiometry was determined in which four hydroxyl groups are involved in the coordination under alkaline conditions. Both studies discussed the possible involvement of hydroxyl groups of the ligand but no experiments were performed dedicated to that issue. In a DFT-study, Birjkumar *et al.* investigated the stability of different binding motifs in UO_2^{2+}–ISA complexes at different pH values.[31] Coordination *via* both oxygens of the carboxylic group (4-membered ring), one oxygen of the carboxylic and one of the α-hydroxy groups (5-membered ring) and one oxygen of the carboxylic and one of the β-hydroxy groups (6-membered ring) was considered. Their calculations revealed that under certain experimental conditions different binding motifs might coexist in solution. However, the involvement of the γ-hydroxy group (C_4–OH) was

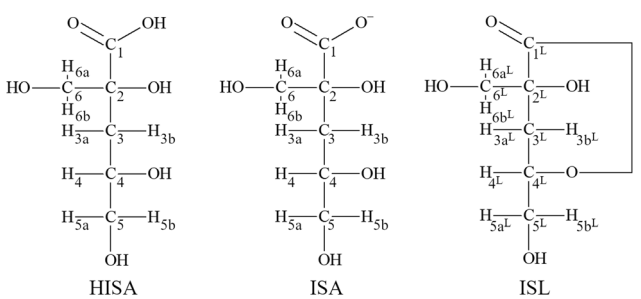

Fig. 1 Structural formula of HISA (α-isosaccharinic acid), ISA (α-isosaccharinate) and ISL (α-isosaccharinate-1,4-lactone) with labelling of protons and carbon atoms.

not considered, which was shown to coordinate to spherical metal centers as mentioned earlier.

It is the aim of the present study to investigate the interaction between ISA and UO_2^{2+}, also as a representative for other actinyl ions, on the molecular level. The focus is on the identification of structural properties of the formed complexes in solution. Since acidic conditions were chosen to avoid the competitive formation of hydrolysis species, the additional question arises whether the presence of the Lewis acidic UO_2^{2+} ion has an impact on the transformation of HISA to ISL. Different complementary spectroscopic and spectrometric techniques were combined with theoretical calculations in order to describe this system from the metal and the ligand point of view.

2 Experimental & methods

2.1 Preparation of a NaISA-stock solution

Preparation of the NaISA-stock solution was performed as described previously.[32,33] 50 g α-lactose monohydrate and 13.6 g $Ca(OH)_2$ were added to 500 mL argon flushed double-distilled (dd) water. The mixture was additionally flushed with argon for 1 h and then carefully sealed. After stirring for 3 days under anaerobic conditions at RT the brown solution was boiled under reflux for 6 h. The hot solution was filtered, and the volume was reduced to 100 mL by boiling. The remaining solution was stored at 4 °C until a white precipitate was formed, which was then filtered and subsequently washed with water and ethanol. After drying at 50 °C, 1.2 g of the crude product was dissolved in 100 mL dd water by boiling and the volume was reduced to 10 mL. The white precipitate was washed twice with water and ethanol and finally dried at 50 °C. In order to exchange Ca^{2+} with Na^+, a cation exchange resin (Chelex® 100, BioRad) was used as described by Van Loon *et al.*[34] An amount of 4 g of the white $Ca(ISA)_2$ was stirred in 100 mL dd water together with 100 g of Chelex-100 resin in the Na^+ form for 3 h. The suspension was centrifuged, and the supernatant was filtered to fully remove the resin. The volume was reduced to 45 mL by boiling, resulting in a brownish solution. The concentration of ISA in the stock solution was determined by total organic carbon (TOC) analysis. Total carbon (TC) and total inorganic carbon (TIC) were determined and the TOC was calculated by subtracting the TIC from the TC. Product purity was confirmed by electrospray-ionization mass spectrometry and nuclear magnetic resonance spectroscopy (section 3.1).

2.2 General sample preparation

For ultraviolet-visible (UV-Vis), electrospray-ionization mass spectrometry (ESI-MS), extended X-ray absorption fine structure (EXAFS) and nuclear magnetic resonance (NMR) measurements a UO_2^{2+}–perchlorate and for attenuated total reflection Fourier-transform infrared (ATR-FTIR) measurements a UO_2^{2+}–chloride stock solution were used. A concentration of 0.1 M for uranium in both stock solutions was determined by ICP-MS. To prepare the UO_2^{2+}–ISA samples, a 0.6 M NaISA stock solution with a pH of 10.5 was used. To adjust the pH, NaOH, $HClO_4$ or HCl were used. The pH was measured with a SenTix Mic electrode (WTW, Germany).

Measurements in different facilities and accompanying transport issues, varying technical efforts as well as different accumulation times to generate evaluable spectra have caused different time spans between preparing the samples and collecting the spectra. The passed times are separately stated for each method in the associated sections below. UV-Vis spectroscopy was used as a reference method to check whether the same dominant species can be expected, if different UO_2^{2+} concentrations and background electrolytes were used, or different waiting times were necessary. An overview of the UV-Vis spectra of the measured UO_2^{2+}-containing samples is shown in ESI section 5.†

2.3 UV-Vis measurements

To determine the number of dominant UO_2^{2+}–ISA species several test series were prepared differing in their molar ratios of UO_2^{2+} and NaISA in solution. The metal-to-ligand (M : L) ratios were 2 : 1, 1 : 1, 1 : 2, 1 : 6 and 1 : 16. While varying the NaISA concentration, the UO_2^{2+} concentration was kept constant at 15 mM. The ionic strength was adjusted to 1 M with $NaClO_4$. The pH-titration experiments were performed as follows: an initial pH was adjusted and the absorption spectrum was immediately recorded. Then, a small amount of NaOH or $HClO_4$ was added to the solution, the pH was measured, and the spectrum was immediately recorded. This procedure was repeated several times. The UV-Vis measurements were performed with a TIDAS 100 spectrometer (J&M Analytik AG, Germany) in a 1 cm quartz cuvette with dd water as the reference with a resolution of 0.1 nm. All spectra were corrected to zero at the lowest absorption of the corresponding spectrum and each test series was individually evaluated with iterative transformation factor analysis (ITFA, additional information are provided in ESI section 8†) between 390 nm and 480 nm.[35]

The method of continuous variation was used to determine the stoichiometry of the formed UO_2^{2+}–ISA species. Therefore, the pH of a 15 mM UO_2^{2+} solution as well as of a 100 mM NaISA solution was adjusted to 4.0. The latter was added to 2 mL of the UO_2^{2+} solution in 40 μL steps. The absorption spectrum was measured immediately after each step as described above.

2.4 Attenuated total reflection Fourier-transform infrared (ATR-FTIR)-spectroscopy

ATR-FTIR spectroscopy can be used to identify structural changes in the ligand due to complex formation, but also in the uranyl moiety by analysis of the bands of the IR active asymmetric stretching vibration of UO_2^{2+}. Measurements were performed as described by Müller *et al.*[36] The ATR-FTIR spectra of aqueous solutions were recorded in the range between 1800 and 700 cm^{-1} on a Bruker Vertex 80/v vacuum spectrometer equipped with a mercury cadmium telluride

(MCT) detector. The spectral resolution was 4 cm^{-1} and spectra were averaged from 256 scans. A horizontal diamond crystal with nine internal reflections (DURA SamplIR II, Smiths Inc.) was used as the ATR accessory. The ATR unit was continuously purged with a current of dry air. To ensure adequate background subtraction, an ATR flow cell was used.

Since relatively large volumes were needed for these measurements, slightly lower concentrations of UO_2^{2+} were used compared to UV-Vis, NMR or EXAFS measurements. A pH series from pH = 1.1 to 4.0 with a fixed molar ratio of UO_2^{2+} (11.25 mM) and NaISA (90 mM) in solution was prepared. Furthermore, a concentration series was prepared at a fixed pH of 4.0. Here, the UO_2^{2+} concentration was constant at 11.25 mM and the M : L ratios were 2 : 1, 3 : 2, 1 : 1, 2 : 3, 1 : 2 and 1 : 4. To identify the spectral changes related to complex formation with UO_2^{2+}, all samples were prepared in the absence and presence of UO_2^{2+}. The concentration of the background electrolyte NaCl was 1 M in all samples and the spectra were recorded one day after preparation.

To assign the spectral changes to certain functional groups, single component spectra of ISL, HISA and ISA were determined, and vibrational modes were assigned to functional groups based on these spectra. To this end, the UO_2^{2+}-free samples of the pH series and an additional sample at pH 9.2 were evaluated with ITFA.

2.5 NMR-spectroscopy

NMR spectra were recorded either on a Varian Inova 400 spectrometer equipped with an AutoX ID probe head with *z*-gradients operating at 399.89 MHz for ^1H or on an Agilent DD2-600 spectrometer equipped with an Agilent One probe operating at 599.80 MHz for ^1H frequency, respectively. For 1D and 2D spectra standard pulse programs were used. D_2O was purchased from Deutero GmbH (Kastellaun, Germany) and used as is. All spectra were referenced to TMSP.

To check the purity of the synthesized NaISA stock solution and to generate the reference data, ^1H, ^{13}C and ^1H,^{13}C-HSQC (heteronuclear single quantum correlation) spectra of 50 mM solutions at pH 2.2, 4.2 and 10.0 were measured immediately after preparation. The sample having a pH of 2.2 was additionally measured after eight days to obtain reliable data for ISL. Samples were prepared by diluting an aliquot of the alkaline NaISA stock solution with D_2O. The pH was adjusted by adding appropriate amounts of $HClO_4$.

To investigate the influence of UO_2^{2+} on the formation of ISL under acidic conditions, two samples were prepared with a NaISA concentration of 60 mM. Solutions were prepared from the alkaline NaISA stock, which contains a fully deprotonated acid (ISA). One of the two samples contained 15 mM UO_2^{2+}. After adjusting the pH to 2.2 (t = 0 min), a series of ^1H-NMR spectra was recorded for both samples until equilibrium was reached (all points in time are listed in Tables SI 6 and 7;† spectra are shown in Fig. SI 19 and 20†). The integrals of the 3a and 3b ^1H-signals of ISL (I_{ISL}) and HISA (I_{HISA}) were used to calculate their relative concentrations by using the following equations.

$$[\mathrm{ISL}]_{\mathrm{rel}} = \frac{I_{\mathrm{ISL}}}{I_{\mathrm{ISL}} + I_{\mathrm{HISA}}}$$

$$[\mathrm{HISA}]_{\mathrm{rel}} = \frac{I_{\mathrm{HISA}}}{I_{\mathrm{ISL}} + I_{\mathrm{HISA}}}$$

To investigate whether the lactone formation has an influence on the speciation of UO_2^{2+}, UV-Vis spectra were obtained from an aliquot of the UO_2^{2+}-containing sample after different points in time.

To determine the dominant binding sites of ISA in the formed UO_2^{2+}–ISA complexes, a sample was prepared containing 15 mM UO_2^{2+} and 30 mM NaISA in D_2O. $HClO_4$ was added until the pH was 4.2. ^1H, ^{13}C and ^1H,^{13}C-HSQC spectra were recorded 1 hour, 3 days and 11 hours after preparation, respectively.

2.6 Electrospray-ionization mass spectrometry (ESI-MS)

ESI-MS was used to determine the composition of UO_2^{2+}–ISA complexes formed in solution as well as to check the purity of the synthesized NaISA stock solution. Measurements were performed with a Velos Pro Orbitrap Elite (Thermo Fisher Scientific Inc., Waltham, MA, USA) using a Nanospray Flex Source. 10 μL of solution were loaded into GlassTip™ emitters from New Objective Inc. (Woburn, MA, USA) and analyzed with an Orbitrap mass analyzer. Full-MS scans from m/z 200 to 2000 were recorded and averaged for 5 minutes. Mass accuracy around 1 ppm was ensured with known lock masses from ambient air. The temperature of the transfer capillary was fixed at 240 °C. All measurements were performed in the positive ionization mode with an applied voltage to the nanospray emitter of 1.8 kV. Four samples were evaluated (six days after preparation), including a NaISA stock solution (15 mM, pH 4) and three UO_2^{2+}–NaISA samples with 1.5 mM UO_2^{2+} and M : L ratios of 2 : 1, 1 : 1 and 1 : 4. Lower UO_2^{2+}-concentrations were used to avoid artefacts in the form of two initially separated molecules measured at their combined mass. The probability of this effect increases with increasing metal and ligand concentrations. Treatment of the data was done with the Xcalibur and Freestyle software from Thermo Fisher.

2.7 DFT calculations

Structure optimizations were performed using the PBE exchange–correlation functional in combination with the TZVPP basis sets for C, N, H and O as implemented in the quantum-chemical program-suite Turbomole, v.7.1.[37–39] For U only the valence electrons were explicitly treated with the TZVPP basis set since a scalar-relativistically corrected 60-electron effective core potential (RECP) was used.[40] The fast and reliable dispersion corrections by Grimme *et al.* as well as the conductor-like screening model (COSMO) with an infinite dielectric constant were used to include dispersion and solvent effects, respectively.[41,42] All structures were identified as minima on the potential energy surface by performing harmonic frequency analyses.

The density difference plot is a helpful tool to identify regions in which electron density is accumulated and depleted during the process of complex formation. The higher the displacement of electrons into bonding regions the stronger the interactions between the respective bonding partners. Calculating a density difference requires a useful decomposition of the complex into single components between which the interactions are to be investigated. The complexes, for which the density difference was calculated, were decomposed while each UO_2^{2+}, each HISA or ISA molecule and the water molecules coordinated to a certain UO_2^{2+} were considered as single components. The electron densities ρ of the whole complex as well as of the single components (with exactly the same coordinates as in the complex) are extracted by single-point calculations with the aforementioned settings (without COSMO) and the electron density difference ρ_{diff} is calculated as:

$$\rho_{diff} = \rho_{complex} - \sum_i \rho_i$$

If ρ_{diff} is positive in a specific region, then the electron density is higher in the complex than in the single components. This is interpreted as an accumulation of electrons during the artificial complex formation. Accordingly, a negative ρ_{diff} shows a depletion of electrons during complex formation.

All representations of optimized structures were created with the Visual Molecular Dynamics (VMD) program version 1.9.3 (http://www.ks.uiuc.edu/Research/vmd/).[43]

A great number of different structures were optimized. The structures were selected according to the different binding motifs that are expected. These include 1 : 1, 2 : 1, 2 : 3 and 1 : 2 UO_2^{2+}–ISA complexes with five- and six-membered rings. The structures shown here are the ones agreeing best with the experimental data. For many of these complexes alternative structures were also optimized. These differed in the direction in which the parts of the ISA molecule that were not directly involved in UO_2^{2+}-coordination were pointing. Such changes did not affect the UO_2^{2+}–ISA binding motif. Whenever possible, the isomer with the lowest energy was chosen.

2.8 Extended X-ray absorption fine structure (EXAFS)

The U L_{III}-edge (17 166 eV) EXAFS spectra of a pH series (pH 1.0 to 4.1, 90 mM of NaISA, 15 mM UO_2^{2+}) and a concentration series (NaISA concentration of 3.5 to 50 mM, pH 3, 15 mM UO_2^{2+}) (Table SI 9†) were recorded (10 to 13 days after preparation) at the Rossendorf Beamline (ROBL) at the European Synchrotron Radiation Facility (ESRF).[44] Higher harmonics were rejected by using two Rh-coated mirrors, while a liquid nitrogen cooled Si(111) double crystal monochromator was used for performing the energy scans in a channel cut mode. For each sample multiple absorption scans were measured with gas filled ionization chambers at room temperature and the Y K-edge (17 038 eV) of a Y metal foil was recorded simultaneously for the calibration of the incident photon energy to the absolute energy scale. In order to increase the signal-to-noise ratio for each sample, four to six scans were measured and averaged. The U L_{III}-edge ionization potential was arbitrarily defined as E_0 = 17 185 eV, whereas the shift in energy threshold (ΔE_0) was defined as a free parameter with $\Delta E_0 = E_0 - E_t$ (E_t – theoretical ionization potential) for the shell fit procedure. The softwares WinXAS (Version 3.11), Sixpack/SamView (Version 0.59) and EXAFSPAK were used for averaging of the multiple sample scans, energy calibration, background subtraction, isolation of the EXAFS signal, and the shell fit.[45–47] For the shell fit, the theoretical scattering phase and amplitude functions were calculated with the *ab initio* scattering code FEFF 8.20 by using a DFT calculated structure of the 2 : 1 UO_2^{2+} : ISA complex, which contains the structural motif of a five- and a six-membered ring (Fig. SI 39†).[48] From each EXAFS sample a UV-Vis spectrum was recorded (immediately and 15 days after preparation), which are depicted in Fig. SI 37.† ITFA was used for the calculation of the qualitative fractionation of the structurally different complexes in the EXAFS and UV-Vis (spectra immediately measured after preparation were used) spectral mixtures (a short description of ITFA is provided in ESI section 8†).[35]

3 Results

3.1 Preparation of NaISA

Since this study focusses on the interaction of UO_2^{2+} with ISA, the discussion of ESI-MS and NMR data of UO_2^{2+}-free NaISA samples, which will be later used as references, was placed in the ESI of this article (ESI section 1†). In conclusion, no impurities were detected in the NaISA stock solution by ESI-MS and NMR spectroscopy.

3.2 NMR spectroscopy

Lactone formation in the presence of UO_2^{2+}. Fig. 1 shows the structural formula of HISA, ISA and ISL with the labelling of protons and carbon nuclei, which will be used to assign ^{1}H- and ^{13}C-NMR signals.

The ^{1}H-signals of the methylene group (C_3) of HISA (3a/3b at 1.93/1.73 ppm) and ISL ($3a^L/3b^L$ at 2.34/2.32 ppm) are well separated and can be used to monitor the lactonization over time (integrated intensities are provided in Tables SI 6 and 7;† ^{1}H-NMR spectra are depicted in Fig. SI 19 and 20†). The transformation of HISA to ISL in the absence and presence of UO_2^{2+} is shown in Fig. 2. The experimental data could be reproduced by using a monoexponential function ($R^2 \geq 99.7\%$), indicating the first-order kinetic behavior of this reaction (all fit results are listed in Table SI 8†). Whether UO_2^{2+} was present or not had no significant effect on the equilibrium concentrations of HISA and ISL (Table SI 8†). In contrast, a crucial impact on the rate constant (k) and consequently on the half-life ($t_{1/2}$) of the lactone formation reaction was observed. In the presence of UO_2^{2+} $t_{1/2}$ decreased from 3294 to 2058 min while k increased from 2.10×10^{-4} to 3.37×10^{-4} min^{-1}. Previous studies from Ekberg *et al.* and Brown *et al.* reported much faster kinetics for the reaction at lower pH, in good agreement with the postulated acid catalyzed reaction mechanism.[20,21]

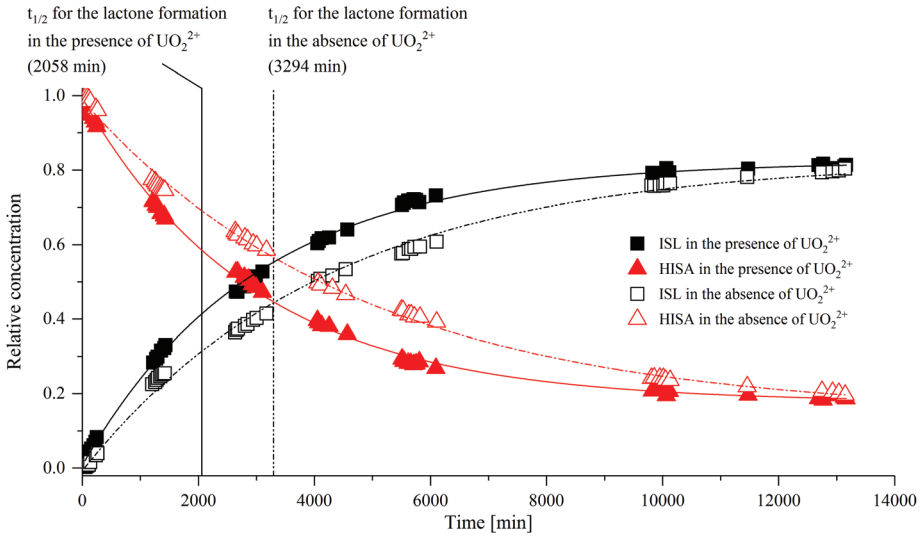

Fig. 2 Influence of UO_2^{2+} on the transformation of HISA to ISL at pH 2.2. Relative concentrations of HISA and ISL were determined based on the ratio of their integrated ^{1}H-NMR signals of 3a/3b and $3a^L/3b^L$ (see section 2.5). Experimental data were fitted with a monoexponential function.

Table 1 Influence of UO_2^{2+} on the positions of ^{1}H-NMR signals of HISA and ISL at pH 2.2

	$\delta(^1H)$ of HISA [ppm]			$\delta(^1H)$ of ISL [ppm]		
Proton	Without UO_2^{2+} [a]	With UO_2^{2+} [b]	$\Delta\delta(^1H)$	Without UO_2^{2+} [a]	With UO_2^{2+} [c]	$\Delta\delta(^1H)$
$3a^{(L)}/3b^{(L)}$	1.93/1.73	2.00/1.81	0.07/0.08	2.34/2.32	2.34/2.31	0.00/−0.01
$4^{(L)}$	3.96	3.98	0.02	4.87	—	—
$5a^{(L)}/5b^{(L)}$	3.55/3.47	3.56/3.48	0.01/0.01	3.92/3.68	3.92/3.68	0.00/0.00
$6a^{(L)}/6b^{(L)}$	3.85/3.59	3.91/3.67	0.06/0.08	3.78/3.72	3.79/3.72	0.01/0.00

[a] Reference data for HISA and ISL were obtained from Table SI 3.† [b] 102 min after preparation. [c] 10 116 min after preparation (proton 4 could not be assigned due to the overlap with the strong water signal); $\Delta\delta$ was calculated by subtracting δ without UO_2^{2+} from δ with UO_2^{2+}.

To identify the origin of the faster reaction kinetics, the positions of ^{1}H-signals of HISA and ISL in the absence and presence of UO_2^{2+} were compared and are summarized in Table 1 (the corresponding spectra are shown in Fig. SI 21–24†). The presence of UO_2^{2+} has no discernable influence on the signals associated with ISL, however shifts could be observed for the HISA signals, suggesting an interaction between the protonated acid and UO_2^{2+}. The values for HISA in the presence of UO_2^{2+} were extracted from the spectrum, which was obtained 102 min after preparation, since the partly overlapping ISL signals were not yet dominant after that relatively short time. However, the spectrum obtained after 10 116 min (Fig. SI 23 and 24†) reveals that the signals corresponding to protons 3a, 3b and 4 of HISA were further shifted downfield to 2.08, 1.90 and 4.00 ppm. This indicates that the exchange of HISA molecules, which are coordinated to UO_2^{2+}, is fast and hence the positions extracted after 102 min are averaged signals of the free and coordinated HISA molecules.

Within the first 10 000 min, in which the HISA concentration considerably changed with increasing time, the absorption spectra of the UO_2^{2+}-containing sample revealed only small changes (Fig. SI 33†). A slightly increased absorption as well as a shift of the initial maximum at 422.3 nm to higher wavelengths occurred. When the equilibrium was almost reached (after 10 000 min) and consequently the HISA concentration remained nearly constant, the absorption spectra did not change. This in combination with the shifted ^{1}H-signals of HISA and the impact on the lactone formation are striking indications that the protonated acid has to be considered, besides ISA, as a ligand for UO_2^{2+}.

Identification of dominant binding sites in UO_2^{2+}–ISA complexes. The dominant binding sites in UO_2^{2+}–ISA complexes shall be identified by comparing the positions of the signals in the presence of UO_2^{2+} (30 mM NaISA; 15 mM UO_2^{2+}; pH 4.2) with signals of the deprotonated ligand (50 mM NaISA; pH 10) in the absence of UO_2^{2+} (Fig. 3). Since the previous results show that the protonated acid cannot be neglected as a ligand, signals for HISA (50 mM NaISA; pH 2.2) were also used as a reference. The interaction of ISA with UO_2^{2+} leads to significant changes in the ^{1}H- and ^{13}C-NMR spectra (see Fig. SI 25 and 26†).

Table 2 summarizes the ^{1}H- and ^{13}C-signals in the absence and presence of UO_2^{2+} as well as the corresponding shifts, which are discussed in this section. Two signals are present in the range, where the signal of the carboxylic carbon was expected. The more intense signal at 191.3 ppm is clearly

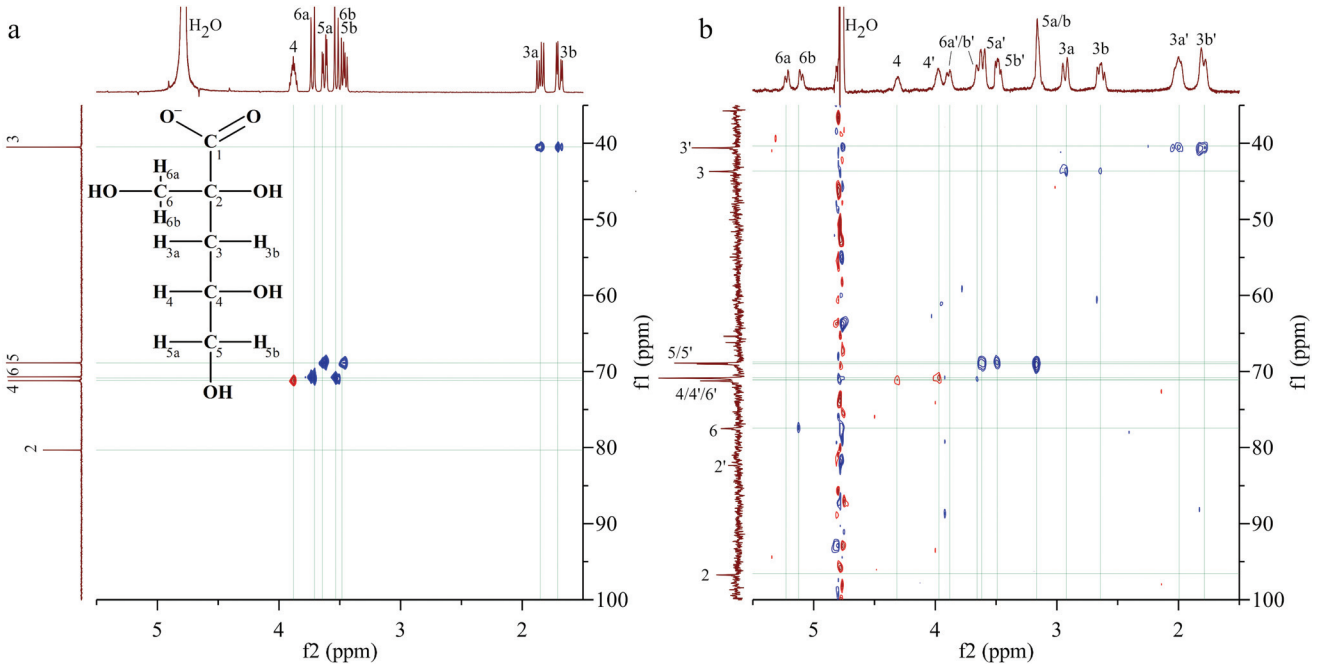

Fig. 3 ^{1}H, ^{13}C-HSQC spectra of (a) the NaISA stock solution (50 mM, pH 10) and (b) a UO_2^{2+}–ISA sample (30 mM NaISA, 15 mM UO_2^{2+}, pH 4.2).

Table 2 Influence of the presence of UO_2^{2+} on the positions of ^{13}C- and ^{1}H-signals at pH 4.2

	$\delta(^{13}C)$ [ppm]			$\delta(^{1}H)$ [ppm]		
Carbon; proton	Reference data ISA[a] and HISA[b]	with UO_2^{2+} (set 1[c] and 2[d])	$\Delta\delta$	Reference data ISA[a] and HISA[b]	with UO_2^{2+} (set 1[c] and 2[d])	$\Delta\delta$
1; —	182.8[a]	191.3[c]	8.5	—	—	—
	180.5[b]	181.4[d]	0.9			
2; —	80.4[a]	96.8[c]	16.4	—	—	—
	79.4[b]	82.4[d]	3.0			
3; 3a/3b	40.5[a]	43.7[c]	3.2	1.85/1.69[a]	2.94/2.66[c]	1.09/0.97
	40.4[b]	40.6[d]	0.2	1.93/1.73[b]	2.01/1.81[d]	0.08/0.08
4; 4	71.2[a]	71.2[c]	0.0	3.88[a]	4.32[c]	0.44
	70.0[b]	70.8[d]	0.8	3.96[b]	3.99[d]	0.03
5; 5a/5b	68.9[a]	69.1[c]	0.1	3.63/3.46[a]	3.17[c]	−0.46/−0.29
	68.7[b]	68.9[d]	0.2	3.55/3.47[b]	3.62/3.50[d]	0.07/0.03
6; 6a/6b	70.9[a]	77.5[c]	6.6	3.72/3.53[a]	5.23/5.13[c]	1.51/1.60
	70.7[b]	70.8[d]	0.1	3.85/3.59[b]	3.90/3.65[d]	0.05/0.06

Reference data for HISA and ISA were obtained from Tables SI 2 and 3;† $\Delta\delta$ was calculated by subtracting a from c and b from d.

shifted by 8.5 ppm, compared to the signal in the absence of UO_2^{2+}. Further assignments are based on the ^{1}H,^{13}C-HSQC spectrum in Fig. 3b. Since the carbon signal at 96.8 ppm shows no correlation with proton signals, it corresponds to carbon 2. A rather weak signal without correlations is present at 82.4 ppm, which is close to the position of carbon 2 in the absence of UO_2^{2+}. The smallest carbon shifts are present at 40.6 and 43.7 ppm, which were consequently assigned to carbon 3. The corresponding proton signals were identified based on the following correlations. Two opposite phased (red) signals must be caused by two spatially differently arranged protons attached to carbon 4. The corresponding carbons show no considerably changed chemical shifts. A pair of doublets, caused by the protons 6a and 6b, which are attached to the carbon of the β-hydroxy group (C_6), is located at 5.23 and 5.13 ppm. The HSQC spectrum shows a correlation of the second signal with the ^{13}C signal at 77.5 ppm, which is consequently carbon 6. Two intense signals result from the coupling of carbon signals at 69.1 and 68.9 ppm with proton signals at 3.62, 3.50 and 3.17 ppm. The carbon shifts match perfectly with the positions of carbon 5 in the absence of UO_2^{2+}. The two remaining proton signals at 3.90 and 3.65 ppm correlate with a carbon signal at 70.8 ppm. These are similar positions for the carbon and protons of position 6 in the absence of UO_2^{2+}.

This analysis revealed that two sets of signals are present for each carbon and proton signal under these experimental conditions, when UO_2^{2+} was in solution. Comparing the ^{1}H-

signals of the set, which is marked with an apostrophe in Fig. 3b (set 2 in Table 2), with reference data for HISA, it becomes apparent that the differences are comparable to those observed earlier in the previous paragraph (Table 1). Therefore, this set can be assigned to HISA interacting with UO_2^{2+}. The shifts of the signals observed for the other set are considerably larger, relative to uncoordinated ISA, indicating a stronger interaction between UO_2^{2+} and ISA compared to HISA. Most significant changes occurred at carbons 1, 2 and 6.

3.3 ATR-FTIR spectroscopy

ATR-FTIR spectroscopy was used as a complementary method for NMR spectroscopy to investigate the structure of ISA in the absence and presence of UO_2^{2+}. Furthermore, the shift of the asymmetric stretching mode of the UO_2^{2+} unit (ν_3) provides information related to the speciation of UO_2^{2+}. To interpret the spectra in the presence of UO_2^{2+} it was necessary to identify the relevant vibrational modes of isosaccharinic acid. Therefore, the UO_2^{2+}-free samples of the pH series including an additional sample at pH 9.2 were measured (spectra are shown in Fig. SI 29† and as dashed lines in Fig. 4b) and evaluated with iterative transformation factor analysis (ITFA). This program is based on principal component analysis and can be used to estimate the number of independent components within a spectroscopic data set as well as to calculate the single component spectra. Furthermore, the distribution of the components within a certain test series can be calculated. A detailed description was given by Rossberg *et al.*[35]

Fig. 4 shows the results of ITFA-evaluation. Three components were necessary to reproduce the measured spectra, the relative distribution of which is shown in Fig. 4a allowing a reasonable assignment to the three possible forms of isosaccharinic acid. ISL dominates under very acidic conditions and gradually transforms to HISA with increasing pH > 1. At higher pH values, HISA is then deprotonated to ISA. Based on the calculated relative concentrations for HISA and ISA between pH 2.8 and 4, a pK_a of 3.6 ± 0.1 was determined, which is comparable to the values reported by Rai and Kitamura.[17] The single component spectra of ISL, HISA and ISA are shown in Fig. 4b and Table 3 summarizes their important vibrational modes (further information concerning the assignments is provided in ESI section 4.2†).

Changes occurring due to the presence of UO_2^{2+} were analyzed based on difference spectra. Therefore, a spectrum of a sample without UO_2^{2+} was subtracted from the corresponding spectrum with UO_2^{2+} while both had the same pH and NaISA concentration. This procedure was, amongst others, described

Table 3 Characteristic vibrational modes of ISL, HISA and ISA

Compound	Wavenumber [cm^{-1}]	Assignment
ISL	1765	ν(C═O)
	1209	ν_{as}(C–O–C)
	1055	ν_{sym}(C–O–C)
HISA	1724	ν(C═O)
	1240	δ(C–OH) + ν(C–OH) (ac)
	1000–1150	ν(C–OH) (alc)
ISA	1583	ν_{as}(COO^-)
	1413	ν_s(COO^-)
	1000–1150	ν(C–OH) (alc)

ac: acid; alc: alcohol; δ: deformation; ν: stretching; as: asymmetric; s: symmetric.

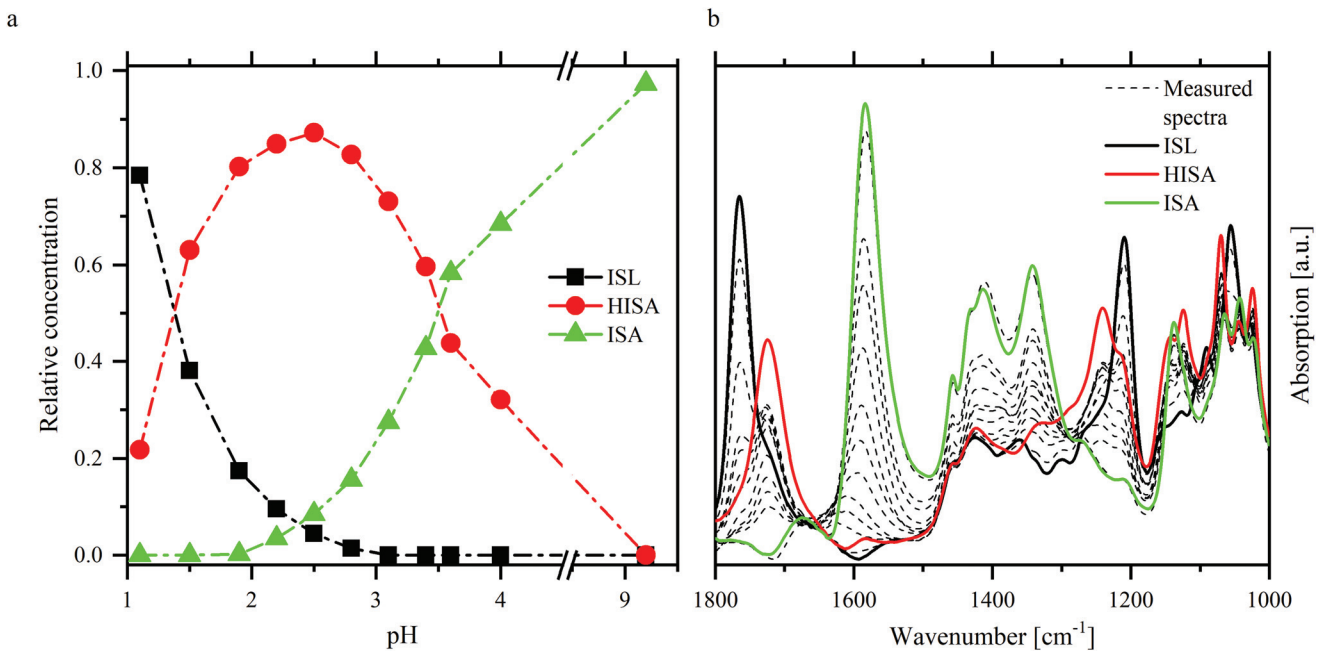

Fig. 4 ITFA evaluation of NaISA ATR-FTIR spectra (90 mM NaISA, 1 M NaCl): distribution of the components (a) and single component spectra (b) of ISL, HISA and ISA.

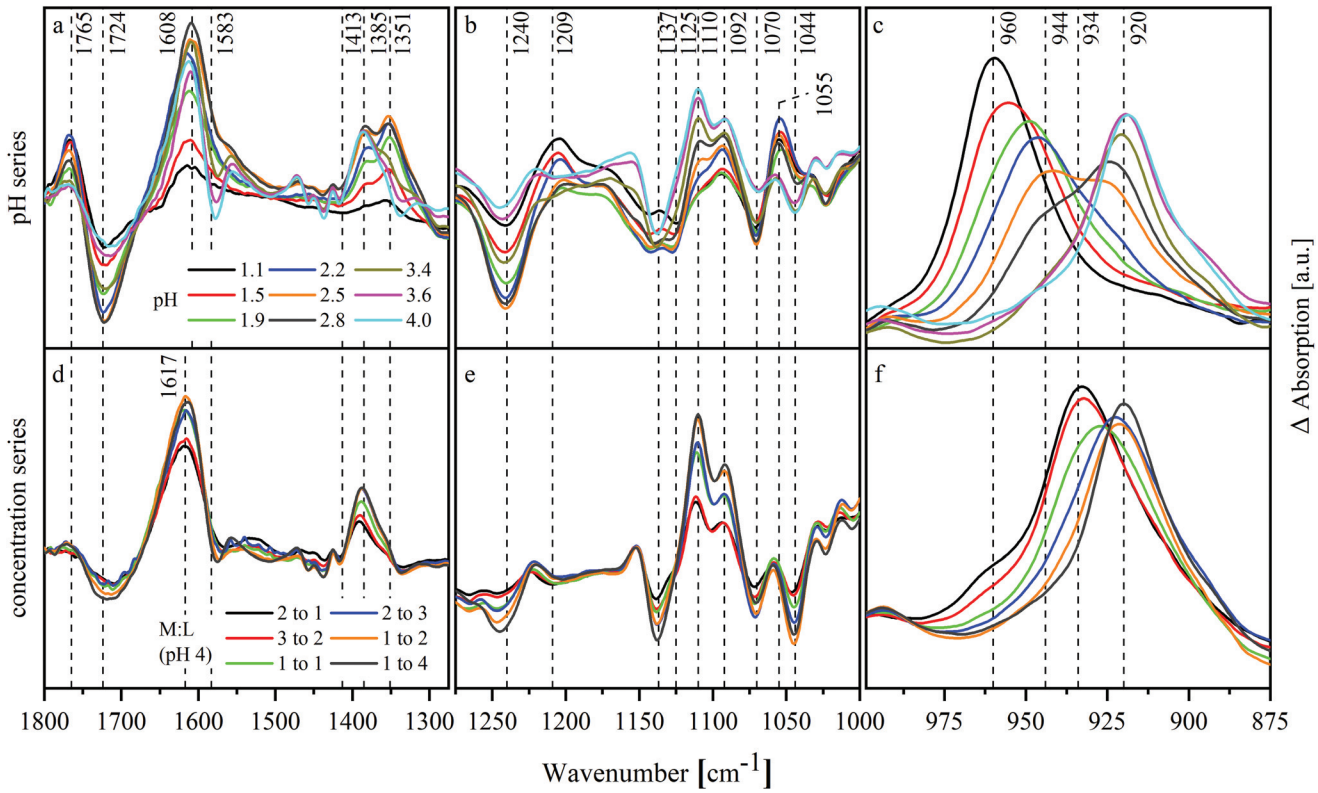

Fig. 5 ATR-FTIR difference spectra of UO_2^{2+}–ISA test series between 1800 cm^{-1} and 875 cm^{-1}: (a, b, c) pH series (11.25 mM UO_2^{2+}, 90 mM NaISA, 1 M NaCl); (d, e, f) concentration series (11.25 mM UO_2^{2+}, pH 4, 1 M NaCl).

by Heller *et al.*[49] The difference spectra of the pH series are shown in Fig. 5a–c and of the concentration series in Fig. 5d–f.

Changes in the spectra, which were caused by the interaction of the ligand with UO_2^{2+} or by the shift of chemical equilibria, occur mainly in the range between 1800 and 1000 cm^{-1} (Fig. 5a, b, d and e). The spectra of the pH series show negative modes at 1724, 1240, 1125 and 1070 cm^{-1} especially below pH 3.4. These modes belong to HISA reflecting a decreased amount of this compound in the presence of UO_2^{2+}. Additionally, positive modes occur in the same pH range at 1765, 1209 and 1055 cm^{-1} corresponding to ISL. This indicates a positive effect of UO_2^{2+} on the lactone formation. The mode at 1351 cm^{-1} correlates with the positive modes of ISL. In the light of the previous results, this mode might be caused by HISA interacting with UO_2^{2+}. Further positive modes occur at 1608, 1385 and 1110 cm^{-1}. Since they are neither present in the spectra of ISL and HISA nor in ISA, they probably originate from UO_2^{2+}–ISA complexes. Their appearance coincides with a shift of the asymmetric stretching of the UO_2^{2+} unit (ν_3) indicating its complexation. The modes at 1608 and 1385 cm^{-1} result from ν_{as} and ν_s of the deprotonated carboxylic group, which were shifted due to the interaction with UO_2^{2+}. Their difference ($\Delta\nu$) increased in the pH series from 170 cm^{-1} in the absence of UO_2^{2+} to 223 cm^{-1} in the presence of UO_2^{2+}.

$\Delta\nu$ in the concentration series is 232 cm^{-1} (ν_{as} at 1617 and ν_s at 1385 cm^{-1}) slightly larger. The positive modes of ISL as well as the mode at 1351 cm^{-1} are not present within this series. Both series show significant changes in the region between 1150 and 1000 cm^{-1} (Fig. 5b and e). Since this is the region where the C–O stretching modes of the alcohol functionalities occur, this indicates their participation in complex formation.

Fig. 5c and f show the shift of ν_3 of the UO_2^{2+} entity. In both series, a shift to lower wavenumbers with increasing pH or mole ratio in solution can be observed reflecting the complex formation. The mode shifts successively from 960 to 944 and finally to 920 cm^{-1} in the pH series. At a mole ratio of 2 : 1 in the concentration series, the mode at 960 cm^{-1} is only present as a shoulder while a mode at 934 cm^{-1} dominates. This mode shifts then to 920 cm^{-1}.

3.4 UV-Vis spectroscopy

UV-Vis spectroscopy was used to estimate the number of dominant UO_2^{2+}–ISA complexes, formed in solution. Therefore, the changes in the absorption spectra of UO_2^{2+}–ISA samples with increasing pH were measured at different mole ratios of UO_2^{2+} to NaISA in solution (M : L = 2 : 1, 1 : 1, 1 : 2, 1 : 6 and 1 : 16). The measured spectra (dashed lines in Fig. 6) were individually evaluated with ITFA. Fig. 6 shows the resulting single component spectra (a–e) and the corresponding distribution of the components (f–j) within the different test series.

Two components (1 and 2) were necessary to reproduce the measured spectra in the first series (M : L = 2 : 1). Increasing

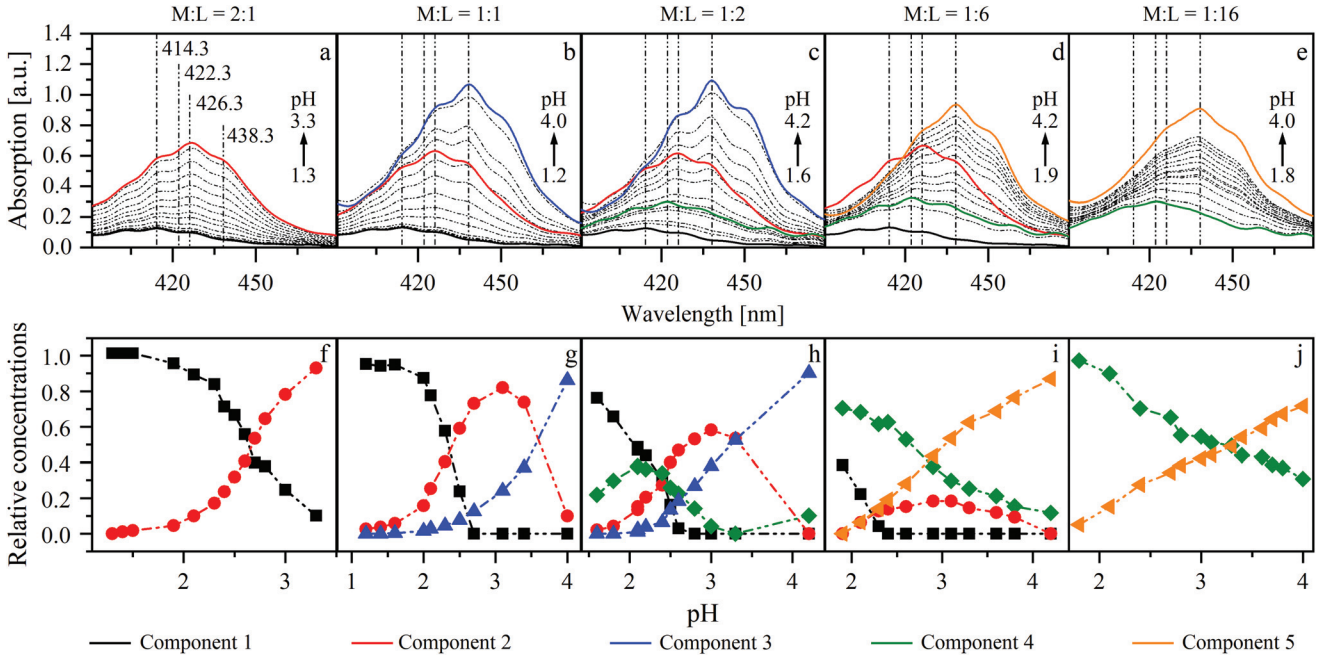

Fig. 6 ITFA evaluation of UV-Vis series at different mole ratios of UO_2^{2+} (15 mM) and ISA in solution (M : L) (a and f = 2 : 1; b and g = 1 : 1; c and h = 1 : 2; d and i = 1 : 6; e and j = 1 : 16). (a–e) Measured spectra (dashed lines) and calculated single component spectra (solid lines); (f–j): calculated relative concentrations of components within a series.

the pH is accompanied by an increased absorption and a shift of the maximum from 414.3 to 426.3 nm (Fig. 6a). The isolated single component spectra of this series were used as references for components 1 and 2 for the evaluation of the test series with M : L ratios of 1 : 1, 1 : 2 and 1 : 6. If ISA and UO_2^{2+} are present in equimolar concentrations, an additional shift from 426.3 to 438.3 nm was observed at higher pH values (Fig. 6b). Therefore, an additional component (3) was necessary to reproduce the measured spectra. Component 4 was needed to describe the spectra of the remaining series, in which the concentration of UO_2^{2+} was lower than that of ISA. The proportion of this component, which has a maximum at 422.3 nm, increases with increasing excess of ISA and simultaneously suppresses the formation of component 2 (Fig. 6c–e). Therefore, at the largest investigated excess (M : L was 1 : 16), again only two components (4 and 5) were necessary to reproduce the measured spectra. The limiting absorption maximum in all series, except the first, is at 438.3 nm. This might emphasize the conclusion that the corresponding components belong to the same chemical species. But the single component spectra of the second and the third series (M : L = 1 : 1 and 1 : 2; Fig. 6b and c) show a larger extinction, compared to the fourth and the fifth series (M : L = 1 : 6 and 1 : 16; Fig. 6d and e). Furthermore, the limiting species were either formed from component 2 or 4. This leads to the conclusion that different limiting species were formed (components 3 and 5), depending on the initial mole ratio.

The averaged single component spectra of all components are shown in Fig. SI 32 (left).† The spectrum of component 1, showing a maximum at 414.3 nm and a corresponding extinction coefficient of 8.5 l mol^{-1} cm^{-1}, is in good agreement with the spectrum of a pure UO_2^{2+} solution without NaISA at pH 2 (Fig. SI 32 right†) and with values reported by Bell and Biggers as well as Meinrath *et al.* for the $[UO_2(H_2O)_5]^{2+}$ complex.[50,51] Therefore, these results suggest the formation of four dominant UO_2^{2+}–ISA complexes. The spectral similarities of components 3 and 5 may be an indication for structural similarities of these species.

UV-Vis spectroscopy was used as an accompanying method for other techniques to check whether the same dominant UO_2^{2+} species can be expected even though different concentrations or mole ratios were used in certain cases. All additional UV-Vis spectra are summarized in ESI section 5.† No additional absorption maxima were observed and spectral developments in the ATR-FTIR as well as EXAFS pH series are comparable to that of the UV-Vis series with a UO_2^{2+} to NaISA mole ratio of 1 to 6 (Fig. 6d). Therefore, the results of the different applied techniques can be complementarily discussed to describe the structural properties as well as formation mechanisms of the formed complexes, since no different dominant species can be expected from the UV-Vis data.

The method of continuous variation, which is commonly known as a Job plot, was used to estimate the stoichiometry in one of the limiting complexes (component 3). This method, which was comprehensively described by Renny *et al.*, was used for that purpose in several other studies.[52–55] In the present case, the absorption maximum of component 3 at 438.3 nm was used. A titration was performed, where a NaISA solution was stepwise added to a UO_2^{2+} solution (for details see section 2.3). The absorption spectra were measured after

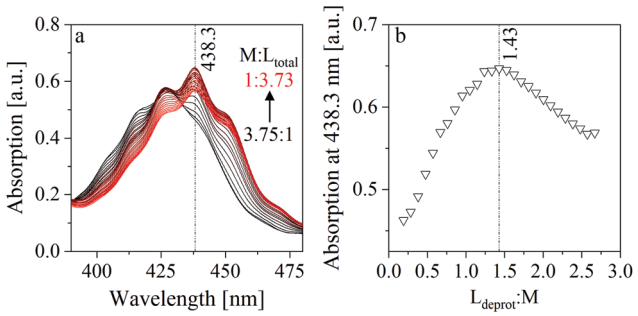

Fig. 7 Method of continuous variation: (a) measured UV-Vis spectra (titration of a 15 mM UO_2^{2+} solution with a 100 mM NaISA solution at pH 4), (b) Job plot (absorption at 438.3 nm plotted against the ratio of deprotonated ligand (L_{deprot}) to UO_2^{2+} (M)).

each step (Fig. 7a) and the absorption at 438.3 nm was plotted against the ratio of the deprotonated ligand in solution (L_{deprot}) to UO_2^{2+} (M) (Fig. 7b). L_{deprot} was calculated based on the pK_a value which was determined from ATR-FTIR measurements (section 3.3). The inflection at 1.43 indicates a stoichiometry of ISA and UO_2^{2+} of 1.5 : 1. Consequently, the stoichiometry in the formed complex is expected to be 2 : 3 (UO_2^{2+} : ISA).

3.5 ESI-MS

Different UO_2^{2+}, ISA and UO_2^{2+}–ISA components were detected by ESI-MS (Fig. SI 38†). For samples 1 and 2 all signals up to 5% of the base peak, whereas for sample 3 all signals up to 2% were considered. To obtain more information concerning the dominant stoichiometries in the formed complexes, the relative proportions of UO_2^{2+} to ISA ratios in the detected compounds were calculated. Therefore, the measured relative intensity of a detected compound was multiplied with the number of containing UO_2^{2+} units. This was then related to the total intensity of all UO_2^{2+}-containing compounds. The results are summarized in Table 4. In the first two samples, where [M] ≥ [L], UO_2^{2+}–ISA compounds with a stoichiometry of 2 : 1 are dominant. The amount of that compound decreased in the third sample, where stoichiometries of 2 : 1, 2 : 3, 1 : 1, and 1 : 2 were present in similar proportions between 17.6 and 26.8%. Considering this and the 2 : 3 complex stoichiometry, which was determined by the method of continuous variation at similar molar ratios of UO_2^{2+} and NaISA in solution (section 3.4), a reasonable explanation may be the fragmentation of the 2 : 3 complex. Even though the ionization process is relatively soft, fragmentation could be caused by the instability of larger complexes in the gas phase and might be further induced by collision with N_2. Consequently, the 1 : 1 and 1 : 2 units can be interpreted as fragments of a 2 : 3 complex, which was initially formed in solution.

Table 4 Relative proportions of detected UO_2^{2+}–ISA compounds in ESI-MS samples

M : L for sample preparation	Relative abundancy of UO_2^{2+}–ISA compounds					
	1 : 0 [%]	2 : 1 [%]	1 : 1 [%]	2 : 3 [%]	1 : 2 [%]	1 : 3 [%]
2 : 1	62.9	34.8	2.3	—	—	—
1 : 1	31.0	56.3	12.7	—	—	—
1 : 4	0	24.0	26.8	17.6	23.9	7.7

3.6 EXAFS

ITFA was applied on the EXAFS spectral mixtures (Fig. SI 42 and Table SI 9†), while the indicator function (IND) was used for the estimation of the number of components, representing structurally different environments of UO_2^{2+}. The IND has a minimum at n = 3 (Table SI 10†), indicating the presence of three dominant components. The VARIMAX procedure results in a qualitative distribution of the components depending on the pH or the NaISA concentration, which is shown in Fig. 8a. However, five components were identified by ITFA based on UV-Vis measurements (section 3.4, Fig. SI 40†) and the resulting relative concentrations within the EXAFS samples are shown in Fig. SI 41.† The different number of detected components can be explained by the different sensitivities of the spectroscopic methods towards structural changes. Since the EXAFS signals depend solely on the atomic near range structure, the lower number of complexes can be caused by structural similarities of certain complexes, which were identified by UV-Vis. Thus, the structurally similar complexes can be identified by comparing the VARIMAX determined distribution of the EXAFS components with the relative concentrations of the components determined by UV-Vis. Only if the UV-Vis determined relative concentrations of components 2 and 4 and of components 3 and 5 are summed, the resulting distribution shows the same trend as observed by the VARIMAX procedure (Fig. 8). Consequently, components 2 and 4 and components 3 and 5 represent complexes with a similar first coordination shell of UO_2^{2+}.

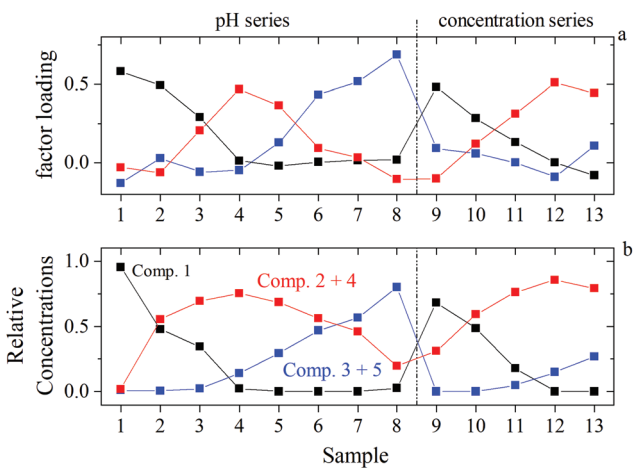

Fig. 8 Identification of structurally similar components by comparing EXAFS and UV-Vis data of identical samples: (a) EXAFS: VARIMAX factor loadings of components 1 (black), 2 (blue), and 3 (red); (b) UV-Vis: ITFA derived relative concentrations of component 1 (black), sum of components 2 and 4 (red), sum of components 3 and 5 (blue) (according to Fig. SI 41†).

Table 5 Shell fit EXAFS structural parameters for components 1 to 3 (* – fixed parameter; / – linked parameter; CN – coordination number; R – radial distance; σ^2 – Debye–Waller factor; ΔE_0 – shift in energy threshold; the standard deviation of the fitted parameters is given in parentheses; amplitude reduction factor S_0^2 = 0.9; multiple scattering paths (MS) ($U–O_{ax1}–U–O_{ax2}$; [a] – literature data from ref. 56)

Component	Shell	CN	R [Å]	σ^2 [Å^2]	ΔE_0 [eV]
1	O_{ax}	2*	1.762(1) 1.764[a]	0.0010(1) 0.0013[a]	3.1(3)
	MS of O_{ax}	/2	/3.524	/0.002	/3.1
	O_{eq}	5.2(3) 5.1[a]	2.414(3) 2.403[a]	0.0073(5) 0.0067[a]	/3.1
2	O_{ax}	2*	1.782(2)	0.0015(2)	1.8(6)
	MS of O_{ax}	/2	/3.564	/0.0030	/1.8
	O_{eq}	4.7(5)	2.364(7)	0.0011(1)	/1.8
3	O_{ax}	2*	1.772(2)	0.0020(2)	3.2(4)
	MS of O_{ax}	/2	/3.544	/0.0040	/3.2
	O_{eq}	4.9(3)	2.380(4)	0.0079(7)	/3.2

In order to isolate the EXAFS spectra of the three components, an iterative target test (ITT, further information is provided in ESI section 8†) was performed by using the UV-Vis determined relative concentrations of the three components, which were kept constant during the iteration. The linear combinations of the isolated spectra weighted by their relative concentrations are in favorable agreement with the measured spectra (Fig. SI 42†), underpinning the validity in the treatment of the UV-Vis data. The shell fits of the isolated spectra and the resulting EXAFS structural parameter are shown in Fig. SI 43† and given in Table 5. The multiple scattering path $U–O_{ax1}–U–O_{ax2}$ (MS of O_{ax}) along the axial O atoms (O_{ax}) was included in the fit, while the radial distance (R) and the Debye–Waller factor (σ^2) was set twice the R and σ^2 of O_{ax}.

In the case of component 1, the structural parameters agree within error with those previously observed for $[UO_2(H_2O)_5]^{2+}$.[56] Hence, component 1 represents the UO_2^{2+} aqua ion. The coordination number (CN) in the equatorial plane (O_{eq}) is five for all components. However, the bond distance $R_{O_{eq}}$ observed for components 2 and 3 (2.36–2.38 Å) is significantly shorter than $R_{O_{eq}}$ of 2.41 Å, measured for $[UO_2(H_2O)_5]^{2+}$. Thus, for components 2 and 3 an interaction with ISA can be assumed. Furthermore, the observed shortening in $R_{O_{eq}}$ is in line with the presence of chelates as dominant binding motifs, in which the ligands coordinate UO_2^{2+} *via* the formation of 5- and 6-membered rings (detailed discussion in section 4.2).[35,57] For components 2 and 3 a feature between 3.35–4.46 Å is present in the Fourier-transform (Fig. SI 43†), which could be explained by various single scattering (SS) and MS events (*e.g.* O_3, $C_{3,4,5}$ and $U–O_1–C_3$, $U–C_1–C_3$, $U–O_2–O_3$, $U–C_2–O_3$ according to Fig. SI 39†). However, it was not shell fitted due to the high number of overlapping scattering effects.

4 Discussion

In a system containing UO_2^{2+} and isosaccharinic acid, the metal center acts as strong Lewis acid while the oxygen atoms of ISA act as Lewis bases. Consequently, the interaction is accompanied by changes in electron density. This was calculated for complexes expected to be formed in solution (further information in section 2.7; figures are shown in ESI section 9† and Fig. 9). Generally, increased electron density is present between U and the coordinating oxygen atoms, which is caused by the electron withdrawing effect of the UO_2^{2+} unit. Additionally, adjacent carbon or proton atoms of the ligand still feel this effect. The coordination of organic ligands in the equatorial plane of the UO_2^{2+} unit decreases the electron density along the $U–O_{yl}$ bond reflecting a weakening of these bonds (causing the shift of $\nu_3(UO_2^{2+})$ towards lower energies observed in the IR spectra, Fig. 5c and f). Furthermore, the two oxygens of the UO_2^{2+}-entity show also an increased electron density, leading to an increased Lewis basicity. This behavior was previously observed for other UO_2^{2+}-ligand systems.[58,59] These changes in the electron distribution within the involved compounds consequently lead to a changed reactivity, which will be further discussed in the following sections.

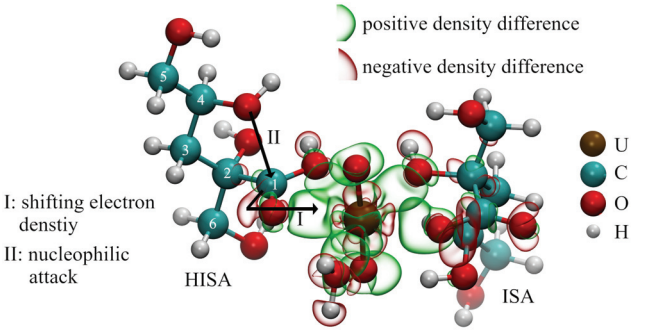

Fig. 9 Calculated electron density changes in a $[UO_2(HISA)(ISA)(H_2O)]^+$ complex and the impact on the lactone formation reaction (isovalues for the representation of electron densities were −0.005 (red) and +0.005 (green).

4.1 Influence of UO_2^{2+} on the lactone formation

^{1}H-NMR spectroscopic measurements revealed the interaction of UO_2^{2+} with HISA at low pH values. Major changes were observed for signals of protons, which are in the surrounding of the carboxylic group (3a/3b and 6a/6b; see Table 1) suggesting a coordination of HISA to UO_2^{2+} in this region. Fig. 9 shows the theoretically calculated electron density changes of a complex involving HISA revealing the previously described general pattern of changing electron density. A clear decrease can be observed between the carboxylic carbon (C_1) of HISA and the corresponding carbonyl oxygen. In other words, this chemical bond is weakened and consequently the corresponding vibrational mode should be shifted to lower wavenumbers. Accordingly, the mode observed at 1351 cm^{-1} in the pH series (Fig. 5a) can be assigned to the stretching vibration of the carbonyl group of HISA coordinated to UO_2^{2+}.

NMR measurements revealed that lactone formation is significantly accelerated in the presence of UO_2^{2+} (Fig. 2) while an effect on the equilibrium concentrations of HISA and ISL was

not observed. The nucleophilic attack of the secondary alcohol (C_4–OH) is likely facilitated by electron withdrawal from the carboxylic carbon (C_1) upon complexation by UO_2^{2+} as shown in Fig. 9, similar to the nucleophilic substitution mechanism postulated for the metal free reaction (Fig. SI 18†). A similar effect was demonstrated by Takao and Akashi showing the promotion of a nucleophilic acyl substitution by a UO_2^{2+} induced carbonyl carbon activation.[55] From this the overall conclusion can be drawn that UO_2^{2+} interacts with HISA and the electrophilic character of U catalyzes the lactone formation reaction under acidic conditions.

4.2 Structural properties of UO_2^{2+}–ISA complexes

The interaction of ISA with UO_2^{2+} causes significant shifts of some ^{13}C signals, which is a consequence of a changed electron density around the corresponding carbon nuclei. The largest shifts were observed for C_1, C_2, and C_6 (Table 2), corresponding to the carboxylic carbon (C_1) as well as the carbons of the α- (C_2–OH) and β-hydroxy group (C_6–OH). All these signals were shifted downfield, which indicates a decreased electron density. This can be traced back to the previously discussed electron withdrawing effect of the UO_2^{2+} entity and therefore reflects the participation of these functional groups in complex formation. Since no considerable shifts were measured for C_4 and C_5, the γ- (C_4–OH) and δ-hydroxy groups (C_5–OH) are not expected to be involved.

ATR-FTIR results add more general information concerning the binding motifs present in UO_2^{2+}–ISA complexes. Changes in the difference between the ν_{as} and ν_s of the carboxylic group, $\Delta\nu$, were often used as a first approximation to describe the coordination behavior in metal–carboxylate complexes.[60–63] A decrease of $\Delta\nu$ compared to the non-coordinated carboxylate anion is associated with a bidentate coordination (both oxygen atoms are coordinated to the metal center) while an increase is associated with a monodentate coordination (only one oxygen is coordinated to the metal center). According to the theoretical investigation of Sutton *et al.*, this behavior can be traced back to different impacts on the geometry of the carboxylic group.[64] Monodentate coordination strongly influences the C–O bond lengths while bidentate coordination particularly affects the O–C–O angle, causing these different changes in $\Delta\nu$. For UO_2^{2+}–ISA the increased $\Delta\nu$ in both, the pH series (+53 cm^{-1}) as well as in the concentration series (+62 cm^{-1}) strongly suggests the monodentate coordination of the carboxylic group. In the case of a bridging motif, where each of the two carboxylate oxygens coordinates to different metal units, it was claimed that $\Delta\nu$ remains constant or behaves like in the case of bidentate coordination. However, Deacon and Phillips also showed examples of asymmetric bridging motifs, where $\Delta\nu$ was increased.[61] Therefore, this motif cannot be excluded at this point. The changes in the region between 1150 cm^{-1} and 1000 cm^{-1} indicate the participation of hydroxy groups in complex formation, which agrees with NMR results. The shortening of the U–O_{eq} bond lengths, which were observed by EXAFS measurements, underpins the conclusion that chelates are formed.

All these findings lead to the conclusion that three binding motifs can be expected in UO_2^{2+}–ISA complexes, which are visualized in Fig. 10: (a) monodentate coordination of the carboxylic and the α-hydroxy group (5-membered ring), (b) monodentate coordination of the carboxylic and the β-hydroxy group (6-membered ring), (c) the carboxylic group acts as a bridge between two UO_2^{2+} units with one UO_2^{2+} additionally binding to the α- and the other UO_2^{2+} binding to the β-hydroxy group (5- and 6-membered rings are simultaneously present).

The binding motifs shown in Fig. 10 agree with the consensus in the literature, that the carboxylic and hydroxy groups coordinate the metal center in concert. Birjkumar *et al.* included the 5- and 6-membered rings as binding motifs in their theoretical study.[31] They concluded that the energy difference between these coordination modes is not sufficient to rule out that both coexist. This agrees with the findings of the present study. Experimental studies related to the structural properties of ISA complexes in general are limited and none was found for UO_2^{2+} or other actinyl ions. Randall *et al.* reported NMR results from studies concerning the identification of functional groups involved in metal coordination.[10] They concluded that both Ca^{2+} and Eu^{3+} form complexes with ISA *via* the carboxylic as well as the α- and γ-hydroxy groups. Similar results were obtained for Ca^{2+} by Dudás *et al.*[26] Apart from the identification of the carboxylic, and α- and γ-hydroxy groups as coordinating functionalities, their NMR results

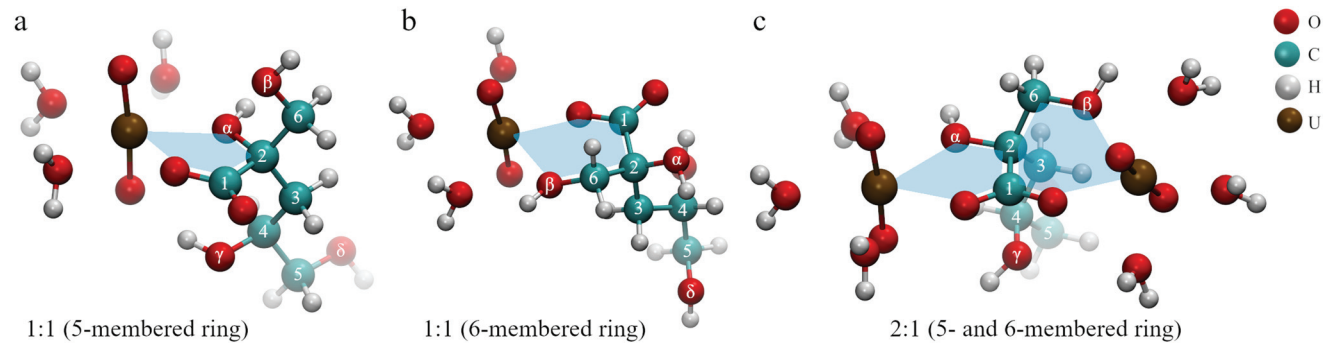

Fig. 10 Dominant binding motifs in UO_2^{2+}–ISA complexes (pictures represent optimized DFT structures): (a) 5-membered ring, (b) 6-membered ring, (c) bridging (5- and 6-membered ring).

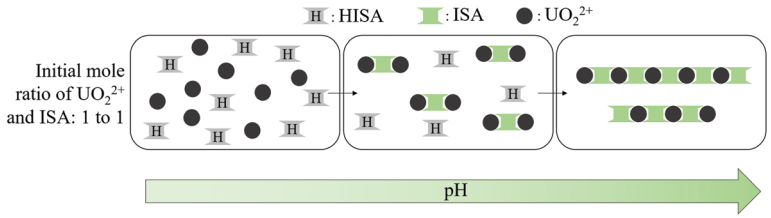

Scheme 1 Simplified complex formation mechanism at equimolar concentrations of UO_2^{2+} and ISA (ISL and coordinated water molecules were neglected for clarity): formation of $[(UO_2)_2(ISA)(H_2O)_6]^{3+}$ complexes in the first and bridging of those in the second step.

showed that the β-hydroxy group is not involved. Tasi *et al.* concluded from DFT optimizations of Pu(IV)–ISA complexes that again the carboxylic, and α- and γ-hydroxy groups are the coordinating functionalities of the ISA molecule.[18] In all described cases, the preference for the α- over the β-hydroxy group is related to the additional binding to the γ-hydroxy group, which is only possible on the side of the α-hydroxy group.

Such a coordination is not feasible for an actinyl moiety, due to its linear O–U–O arrangement. The γ-hydroxy group cannot bind to the uranium at the same time as the carboxylic group and instead can form a hydrogen bond with one of the UO_2^{2+} oxygen atoms, which can be seen in Fig. 10a. Consequently, the energetic difference between the 5-membered ring involving the α-hydroxy group and the 6-membered ring involving the β-hydroxy group is negligible for UO_2^{2+}, which can explain the coexistence of the two binding sites. The bridging motif in Fig. 10c cannot be directly proven based on NMR or ATR-FTIR data, as it is essentially both motifs shown in Fig. 10a and b occurring in the same molecule. The experimentally determined complex stoichiometries of 2 : 1 and 2 : 3, however, suggest the presence of such a bridging motif in these binuclear complexes. Furthermore, the presence of two binding sites for each ISA molecule is the key information to understand the mechanisms on a molecular level.

4.3 Complex-formation mechanism

Both UV-Vis and ATR-FTIR measurements suggested the formation of different species depending on the mole ratio of UO_2^{2+} and ISA in solution. If a twofold excess of UO_2^{2+} was present, a species showing an absorption maximum at 426.3 nm and a asymmetric stretching mode of the UO_2^{2+} (ν_3) unit at 934 cm^{-1} was formed in solution (Fig. 5f and 6a/f). Furthermore, Fig. 6f shows that the initially present UO_2^{2+} was almost completely transformed into that compound. Considering that each ISA molecule can bind two UO_2^{2+} cations, the metal-to-binding site ratio is 1 : 1, if the molar ratio of UO_2^{2+} and NaISA is 2 : 1. This suggests that complexes with the stoichiometry 2 : 1 (UO_2^{2+} : ISA) were formed. This hypothesis is confirmed by the ESI-MS measurements, which show that a 2 : 1 stoichiometry dominates the complex species for samples showing the absorption maximum at 426.3 nm in UV-Vis experiments (Table 4 and Fig. SI 36†). According to the general conclusion from EXAFS measurements that the coordination number of the UO_2^{2+} unit was slightly larger than five for all compounds, the initially formed species under these conditions can be written as $[(UO_2)_2(ISA)(H_2O)_6]^{3+}$, whose structure is shown in Fig. 10c (and Fig. SI 50/51†).

These initially formed $[(UO_2)_2(ISA)(H_2O)_6]^{3+}$ complexes can be bridged by additional ISA molecules, if enough ligand molecules are present in solution, leading to the formation of polynuclear chains. Such a chain-like pattern was observed in the structure of $[UO_2(C_2O_4)_2H_2O]\cdot 2H_2O$.[65] This process is shown in Scheme 1. The additional coordination of a second ISA molecule in the equatorial plane of UO_2^{2} can be recognized by a further shift of $\nu_3(UO_2^{2+})$ to 920 cm^{-1} as well as an additional component in the UV-Vis spectra with an absorption maximum at 438.3 nm (Fig. 5f and 6b/g). Consequently, the species formed under these conditions can be assigned to complexes with the general formula $[(UO_2)_m(ISA)_n(H_2O)_x]^{2m-n}$ (with $m > 2$ and $n = m + 1$, m or $m - 1$).

If the initial amount of ISA exceeds that of UO_2^{2+}, the formation of a different species suppresses the formation of the $[(UO_2)_2(ISA)(H_2O)_6]^{3+}$ complex at low pH values. This can be clearly seen in Fig. 6h–j and c–e, in which component 4 becomes more dominant with increasing excess of NaISA. As described in section 4.1, HISA is also able to coordinate to UO_2^{2+}. Therefore, the suppressed formation of polynuclear species at lower pH values can be traced back to the interaction of HISA with UO_2^{2+} as the competing process. In other words, the higher the amount of HISA present in solution the more is the formation of polynuclear chains suppressed and smaller molecules are formed. This is in agreement with the complex-stoichiometry of 2 to 3 suggested from the method of continuous variation and ESI-MS measurements at higher initial concentrations of ISA compared to UO_2^{2+} in solution (Fig. 7 and Table 4). An optimized structure of such a $[(UO_2)_2(ISA)_3(H_2O)_2]^{+}$ complex (2 : 3) is shown in Fig. 11a. The absorption spectra of the EXAFS- and ATR-FTIR pH series show a maximum at 414.3 nm at the lowest pH (1.1) (Fig. SI 35 left and 37 left†) corresponding to the $[UO_2(H_2O)_5]^{2+}$ complex. Since HISA and ISL dominate at pH 1.1, the species showing the absorption at 422.3 nm and $\nu_3(UO_2^{2+})$ at 944 cm^{-1}, most likely includes a stronger complexing ISA molecule. Consequently, the initially formed species under conditions where the initial concentration of ISA in solution strongly exceeds that of UO_2^{2+} can be assigned to a $[UO_2(ISA)(H_2O)_3]^{+}$ complex (1 : 1), while some of the water molecules can be exchanged by one or more HISA molecules. An optimized structure with one attached HISA molecule is shown in Fig. 9

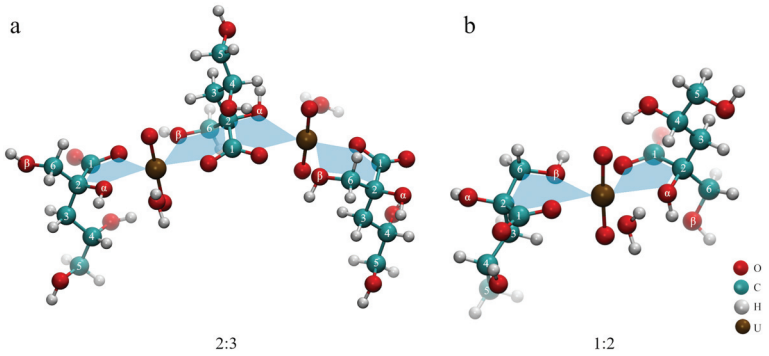

Fig. 11 Optimized structures of 2 : 3 (a) and 1 : 2 (b) UO_2^{2+}–ISA complexes.

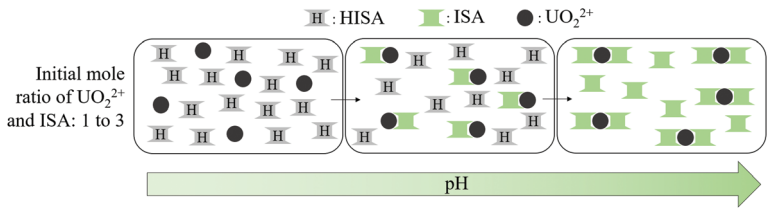

Scheme 2 Simplified complex formation mechanism at an excess of ISA (ISL and coordinated water molecules were neglected for clarity): formation of $[UO_2(ISA)(H_2O)_3]^+$ complexes (the formation of polynuclear complexes is inhibited by interaction with HISA molecules) in the first and $[UO_2(ISA)_2(H_2O)]$ complexes in the second step.

and Fig. SI 52.† Once this species is formed and the pH is increased, the attached HISA molecule gets deprotonated leading to the formation of $[UO_2(ISA)_2(H_2O)]$ complexes (1 : 2). This mechanism is shown in Scheme 2. The optimized structure of a $[UO_2(ISA)_2(H_2O)]$ complex showing a 5- and 6-membered ring as a binding motif is shown in Fig. 11b.

The UO_2^{2+} units in the polynuclear complexes $[(UO_2)_m(ISA)_n(H_2O)_x]^{2m-n}$ and also in the $[UO_2(ISA)_2(H_2O)]$ complex have two binding partners in their equatorial plane. These structural similarities provide a reasonable explanation for their spectroscopic similarities in terms of absorption maxima and position of $\nu_3(UO_2^{2+})$. This conclusion was supported by the combination of EXAFS and UV-Vis spectroscopy (see section 3.6). Components 3 and 5, which correspond to the polynuclear $[(UO_2)_m(ISA)_n(H_2O)_x]^{2m-n}$ and the $[UO_2(ISA)_2(H_2O)]$ complexes, represent two species in the UV-Vis spectra but cannot be distinguished by EXAFS. The five dominant components identified in the present study, their assignments as well as their spectral properties are summarized in Table 6.

The lactone form of the ligand has no direct impact on the complex formation, other than reducing the amount of HISA available for the interaction with UO_2^{2+} at low pH. This subtle effect of lactone formation can be seen in Fig. SI 37,† showing the UV-Vis spectra of the EXAFS samples measured immediately and 15 days after preparation. The extinction is slightly increased while the absorption maxima remain constant. A similar effect was observed for the UV-Vis spectra of the long-term lactone formation NMR-experiment (Fig. SI 33†). Furthermore, the absorption maximum slightly shifted from 422.3 nm, corresponding to $[UO_2(ISA)(H_2O)_3]^+$ associated with HISA, to higher wavelengths. According to the previously discussed complex formation mechanisms, the formation of polynuclear species (having their maxima at 426.3 and 438.3 nm)

Table 6 Assignments and spectral properties of identified UO_2^{2+}–ISA complexes

Component	Assigned complex	Absorption maximum [nm] (ε [l·mol^{-1}·cm^{-1}])	$\nu_3(UO_2^{2+})$ [cm^{-1}]
1	$[UO_2(H_2O)_5]^{2+}$	414.3 (8.5)	960
2	$[(UO_2)_2ISA(H_2O)_6]^{3+}$	426.3 (42.8)	934
3	$[(UO_2)_m(ISA)_n(H_2O)_x]^{2m-n}$ [a] $[(UO_2)_2(ISA)_3(H_2O)_2]^+$	438.3 (72.0)	920
4	$[UO_2(ISA)(H_2O)_3]^+$ [b]	422.3 (20.5)	944
5	$[UO_2(ISA)_2(H_2O)]$	438.3 (61.4)	920

[a] $m > 2$, $n = m + 1$, m or $m - 1$. [b] Associated with one or more weakly bound HISA molecules.

was less suppressed in the NMR-experiment with increasing time causing the observed spectral changes. Since the same absorption maxima were observed and the previously mentioned changes in the UV-vis spectra are rather small, no impact of the lactone formation on the dominant species formed in solution is observed. However, the kinetic aspect of the lactone formation has to be appropriately considered, if the experiments are intended to determine complex formation constants.

4.4 Comparison with literature data for the UO_2^{2+}–ISA system

Warwick *et al.* characterized complexes between selected divalent metals (Cd^{2+}, Co^{2+} and UO_2^{2+}) and ISA under near-neutral and alkaline conditions.[30] Furthermore, the stoichiometries of metals, hydroxide ions and ISA molecules as well as stability constants for the identified species were determined. The ratio of metal ions and ISA molecules in the formed complexes was determined by conductometric titrations. The procedure of this particular experiment was the same for all investigated metals. For that purpose, 1 mL aliquots of a 0.1 M metal chloride solution, which corresponds to 0.1 mmol of metal per aliquot, were stepwise added to 20 mL of a 0.1 M NaISA solution, which corresponds to 2 mmol ISA. The conductivity was measured after each titration step. Changes in the gradient of the measured conductance and the corresponding volume of the added metal solution were then used to derive the stoichiometry. For Cd and Co, inflexions were observed at 20 mL added metal solution corresponding to 2 mmol of metal. Consequently, equimolar concentrations of ISA and metal were present at this point leading to the conclusion that the stoichiometry of the formed complex between Cd and Co with ISA is 1 to 1. The same ratio was proposed for UO_2^{2+} even though the inflexion in the conductance was already observed at 10 mL of added metal solution. This corresponds to 1 mmol of UO_2^{2+} giving a metal to ligand ratio of 1 : 2 (1 mmol UO_2^{2+} to 2 mmol ISA) at this point. This result is in line with one of the proposed species identified in the present study, which was formed when ISA is present in excess.

Another study was performed by Rao *et al.*, where the UO_2^{2+}–ISA system was characterized under acidic conditions by potentiometry and calorimetry.[29] They determined the formation of three complexes with UO_2^{2+} to ISA ratios of 1 to 1, 1 to 2 and 1 to 3. Even though the experiments were performed in a similar concentration range, no indication was found for the latter complex in the present study. A possible explanation for that apparent discrepancy may be found in the data evaluation approach. The average number of ISA molecules bound to UO_2^{2+} ($\bar{n}$) from potentiometric data was calculated by the following equation:

$$\bar{n} = \frac{\{C_L - [L^-](1 + K_H[H^+])\}}{C_M}.$$

In this approach, the acid constant (K_H) for HISA was assumed to be a constant. Our results, however, clearly show the interaction between UO_2^{2+} and HISA. The electron withdrawal from the protonated carboxylic group may increase the acidity of the proton. Larger values for K_H would in turn lead to smaller values for $\bar{n}$. The potentiometric analysis would then require a correction for this effect. This emphasizes the requirement, if possible, for the combination of potentiometry with spectroscopic techniques as complementary methods.

5 Conclusion

The present work highlights the complex interaction of mutual influence on the chemical speciation of metals and ligands. Only by the collective interpretation of data of a number of complementary analytical methods, it was possible to understand the interaction of UO_2^{2+} and isosaccharinic acid on the molecular level. This approach allows the characterization of the system from the metal and the ligand point of view. This study shows that (1) ISA is able to bridge UO_2^{2+} units under certain experimental conditions and (2) UO_2^{2+} interacts with the protonated form of the ligand, which changes its chemical reactivity, and in turn affects the complex formation mechanism. These findings for the first time give a complete picture of the interaction of UO_2^{2+} with ISA over a wide range of solution compositions and extend the understanding of UO_2^{2+} interaction with organic compounds.

On the basis of the reaction mechanisms and complex stoichiometries determined in this study, thermodynamic data for the complex formation process can be determined, either by new experiments or by reevaluation of the existing data. In this process, the kinetic effect of the ISL–HISA–ISA equilibrium altered by the presence of UO_2^{2+} can also be considered. This will have a significant impact on the reliability of the assessment of the impact of ISA on the mobility of UO_2^{2+} and other actinyl ions in the context of nuclear waste disposal research.

Conflicts of interest

There are no conflicts of interest to declare.

Acknowledgements

This project has received funding from the Euratom research and training programme 2014–2018 under Grant Agreement no. 61880. Manuel Raiwa acknowledges the financial support by the German Federal Ministry of Education and Research (BMBF) in the joint project SIRIUS (02NUK044A). The authors would like to acknowledge Carola Eckardt for TOC measurements. We also thank Moritz Schmidt for proofreading the article.

References

1 U. R. Berner, *Waste Manag.*, 1992, **12**, 201–219.
2 M. H. Bradbury and L. R. Van Loon, *Cementitious Near-Field Sorption Data Bases for Performance Assessment of a L/ILW Repository in a Paifris Marl Host Rock*, 1997, vol. PSI-Berich.

3 L. Abrahamsen, T. Arnold, H. Brinkmann, N. Leys, M. Merrous, K. Mijnendonckx, H. Moll, P. Polvika, J. Sevcu, J. Small, M. Vikman and K. Wouters, *A review of anthropogenic organic wastes and their degradation behaviour*, 2015.
4 M. A. Glaus and L. R. Van Loon, *Environ. Sci. Technol.*, 2008, **42**, 2906–2911.
5 I. Pavasars, J. Hagberg, H. Borén and B. Allard, *J. Polym. Environ.*, 2003, **11**, 39–47.
6 M. Glaus, L. R. Van Loon, S. Achatz, A. Chodura and K. Fischer, *Anal. Chim. Acta*, 1999, **398**, 111–122.
7 L. R. Van Loon and M. A. Glaus, *J. Environ. Polym. Degrad.*, 1997, **5**, 97–109.
8 P. N. Humphreys, A. Laws and J. Dawson, *A Review of Cellulose Degradation and the Fate of Degradation Products Under Repository Conditions*, 2010, vol. 001.
9 L. R. Van Loon, M. A. Glaus, A. Laube and S. Stallone, *Radiochim. Acta*, 1999, **86**, 183–189.
10 M. Randall, B. Rigby, O. Thomson and D. Trivedi, *Assessment of the effects of cellulose degradation products on the behaviour of europium and thorium*, 2013.
11 G. M. N. Baston, J. A. Berry, K. A. Bond, K. A. Boult, M. Brownsword and C. M. Linklater, *J. Alloys Compd.*, 1994, **213–214**, 475–480.
12 G. M. N. Baston, J. A. Berry, K. A. Bond, K. A. Boult and C. M. Linklater, *Radiochim. Acta*, 1994, **66–67**, 437–442.
13 G. M. N. Baston, M. M. Cowper, T. G. Heath, T. A. Marshall and S. W. Swanton, *Mineral. Mag.*, 2012, **76**, 3381–3390.
14 L. R. Van Loon and M. A. Glaus, *Experimental and Theoretical Studies on Alkaline Degradation of Cellulose and its Impact on the Sorption of Radionuclides*, 1998.
15 W. Hummel, G. Anderegg, L. Rao, I. Puigdomènech and O. Tochiyama, *Chemical Thermodynamics Of Compounds And Complexes Of U, Np, Pu, Am, Tc, Se, Ni and Zr With Selected Organic Ligands*, 2005.
16 X. Gaona, V. Montoya, E. Colàs, M. Grivé and L. Duro, *J. Contam. Hydrol.*, 2008, **102**, 217–227.
17 D. Rai and A. Kitamura, *J. Chem. Thermodyn.*, 2017, **114**, 135–143.
18 A. Tasi, X. Gaona, D. Fellhauer, M. Böttle, J. Rothe, K. Dardenne, R. Polly, M. Grivé, E. Colàs, J. Bruno, K. Källström, M. Altmaier and H. Geckeis, *Appl. Geochem.*, 2018, **98**, 247–264.
19 A. Tasi, X. Gaona, D. Fellhauer, M. Böttle, J. Rothe, K. Dardenne, R. Polly, M. Grivé, E. Colàs, J. Bruno, K. Källstrom, M. Altmaier and H. Geckeis, *Appl. Geochem.*, 2018, **98**, 351–366.
20 P. L. Brown, S. Allard and C. Ekberg, *J. Chem. Eng. Data*, 2010, **55**, 5207–5213.
21 S. Ekberg, C. Ekberg and Y. Albinsson, *J. Solution Chem.*, 2004, **33**, 465–477.
22 H. Cho, D. Rai, N. J. Hess, Y. Xia and L. Rao, *J. Solution Chem.*, 2003, **32**, 691–702.
23 D. Rai, N. J. Hess, Y. Xia, L. Rao, H. M. Cho, R. C. Moore and L. R. Van Loon, *J. Solution Chem.*, 2003, **32**, 665–689.
24 D. Rai and A. Kitamura, *J. Nucl. Sci. Technol.*, 2016, **53**, 459–467.
25 K. Vercammen, M. A. Glaus and L. R. Van Loon, *Radiochim. Acta*, 2001, **89**, 393–401.
26 C. Dudás, B. Kutus, É. Böszörményi, G. Peintler, Z. Kele, I. Pálinkó and P. Sipos, *Dalton Trans.*, 2017, **46**, 13888–13896.
27 M. R. González-Siso, X. Gaona, L. Duro, M. Altmaier and J. Bruno, *Radiochim. Acta*, 2018, **106**, 31–45.
28 E. Colàs Anguita, PhD thesis, Universitat Politècnica de Catalunya, 2014, http://hdl.handle.net/2117/95404.
29 L. Rao, A. Y. Garnov, D. Rai, Y. Xia and R. C. Moore, *Radiochim. Acta*, 2004, **92**, 575–581.
30 P. Warwick, N. Evans and S. Vines, *Radiochim. Acta*, 2006, **94**, 363–368.
31 K. H. Birjkumar, N. D. Bryan and N. Kaltsoyannis, *Dalton Trans.*, 2012, **41**, 5542.
32 L. R. Whistler and J. N. BeMiller, in *Methods in carbohydrate chemistry*, 1963, vol. 2, pp. 477–479.
33 N. M. Bassil, N. Bryan and J. R. Lloyd, *ISME J.*, 2015, **9**, 310–320.
34 L. R. Van Loon, M. A. Glaus, S. Stallone and A. Laube, *Environ. Sci. Technol.*, 1997, **31**, 1243–1245.
35 A. Rossberg, T. Reich and G. Bernhard, *Anal. Bioanal. Chem.*, 2003, **376**, 631–638.
36 K. Müller, V. Brendler and H. Foerstendorf, *Inorg. Chem.*, 2008, **47**, 10127–10134.
37 J. P. Perdew, K. Burke and M. Ernzerhof, *Phys. Rev. Lett.*, 1996, **77**, 3865–3868.
38 A. Schäfer, C. Huber and R. Ahlrichs, *J. Chem. Phys.*, 1994, **100**, 5829–5835.
39 TURBOMOLE GmbH, *Turbomole*, 2016.
40 X. Cao and M. Dolg, *J. Mol. Struct. (THEOCHEM)*, 2004, **673**, 203–209.
41 S. Grimme, J. Antony, S. Ehrlich and H. Krieg, *J. Chem. Phys.*, 2010, **132**, 154104.
42 A. Klamt and G. Schüürmann, *J. Chem. Soc., Perkin Trans. 2*, 1993, 799–805.
43 W. Humphrey, A. Dalke and K. Schulten, *J. Mol. Graphics*, 1996, **14**, 33–38.
44 T. Reich, G. Bernhard, G. Geipel, H. Funke, C. Hennig, A. Rossberg, W. Matz, N. Schell and H. Nitsche, *Radiochim. Acta*, 2000, **88**(9–11), 633–637.
45 T. Ressler, *J. Synchrotron Radiat.*, 1998, **5**, 118–122.
46 S. M. Webb, *Phys. Scr.*, 2005, 1011.
47 G. N. George and I. J. Pickering, *EXAFSPAK: A Suite of Computer Programs for Analysis of X-ray Absorption Spectra, Stanford Synchrotron Radiation Laboratory*, Stanford, CA, USA, 1995.
48 A. L. Ankudinov, B. Ravel, J. J. Rehr and S. D. Conradson, *Phys. Rev. B: Condens. Matter Mater. Phys.*, 1998, **58**, 7565–7576.
49 A. Heller, A. Barkleit, H. Foerstendorf, S. Tsushima, K. Heim and G. Bernhard, *Dalton Trans.*, 2012, **41**, 13969–13983.
50 J. Bell and R. Biggers, *J. Mol. Spectrosc.*, 1965, **18**, 247–275.
51 G. Meinrath, D. Kwiatek, Z. Hnatejko and S. Lis, *Monatsh. Chem. - Chem. Mon.*, 2014, **145**, 1689–1696.

52 J. S. Renny, L. L. Tomasevich, E. H. Tallmadge and D. B. Collum, *Angew. Chem., Int. Ed.*, 2013, **52**, 11998–12013.
53 D. Kim, K. Park, M. Yang, T. Kim, R. Mahajan and J. Kim, *Talanta*, 2007, **74**, 223–228.
54 S. Bashir, S. R. Maqsood, G. M. Peerzada, B. Khan and M. A. Rizvi, *J. Inorg. Chem.*, 2014, **2014**, 1–11.
55 K. Takao and S. Akashi, *RSC Adv.*, 2017, **7**, 12201–12207.
56 C. Lucks, A. Rossberg, S. Tsushima, H. Foerstendorf, A. C. Scheinost and G. Bernhard, *Inorg. Chem.*, 2012, **51**, 12288–12300.
57 L. Rao, J. Jiang, P. Zanonato, P. Di Bernardo, A. Bismondo and A. Y. Garnov, *Radiochim. Acta*, 2002, **90**, 581–588.
58 M. J. Sarsfield and M. Helliwell, *J. Am. Chem. Soc.*, 2004, **126**, 1036–1037.
59 N. Miyamoto, T. Tsukahara and Y. Ikeda, *Chem. Lett.*, 2012, **41**, 513–515.
60 T. J. Strathmann and S. C. B. Myneni, *Geochim. Cosmochim. Acta*, 2004, **68**, 3441–3458.
61 G. Deacon and R. J. Phillips, *Coord. Chem. Rev.*, 1980, **33**, 227–250.
62 M. B. Hay and S. C. B. Myneni, *Geochim. Cosmochim. Acta*, 2007, **71**, 3518–3532.
63 M. Kakihana, T. Nagumo, M. Okamoto and H. Kakihana, *J. Phys. Chem.*, 1987, **91**, 6128–6136.
64 C. C. R. Sutton, G. da Silva and G. V. Franks, *Chem. – Eur. J.*, 2015, **21**, 6801–6805.
65 J. Leciejewicz, N. W. Alcock and T. J. Kemp, in *Coordination Chemistry*, Springer-Verlag, Berlin/Heidelberg, 1995, vol. 82, pp. 43–84.